High Lithium Ion Electroinsertion Rate into Self-Assembled Films Formed from TiO2

ARTICLE *in* THE JOURNAL OF PHYSICAL CHEMISTRY C · AUGUST 2013

Impact Factor: 4.77 · DOI: 10.1021/jp404179x

THE JOURNAL OF PHYSICAL CHEMISTRY C

Article

pubs.acs.org/JPCC

High Lithium Ion Electroinsertion Rate into Self-Assembled Films Formed from TiO_2

Wellington J. A. S. Gomes,[†] Diógenes M. Araújo,[†] Antonio J. F. Carvalho,[‡] Sergio P. Campana-Filho,[§] and Fritz Huguenin*[,†]

[†]Departamento de Química, Faculdade de Filosofia, Ciências e Letras de Ribeirão Preto, Universidade de São Paulo, 14040-901 Ribeirão Preto (SP), Brazil

[‡]Deparamento de Engenharia de Materiais, Escola de Engenharia de São Carlos, Universidade de São Paulo, 13566-590 São Carlos (SP), Brazil

[§]Instituto de Química de São Carlos, Universidade de São Paulo, 13560-970 São Carlos (SP), Brazil

Supporting Information

ABSTRACT: We prepared self-assembled materials consisting of TiO_2 nanoparticles, *N*,*O*-carboxymethylchitosan (NOCMCh), and poly(ethylene oxide) (PEO) by the layer-by-layer (LbL) technique, aiming to employ them as modified electrodes under high lithium ion electroinsertion rate. Electrostatic interaction between the components promoted growth of visually uniform TiO_2/NOCMCh films with highly controlled thickness. We used NOCMCh to produce a polymeric mixture with PEO to incorporate the polyether into the self-assembled structure during the preparation of the LbL TiO_2/NOCMCh/PEO films. Scanning electron microscopy (SEM) and contact angle measurements between the electrolytic solution and the thin films surface suggested that the polymers affected the mean size of the aggregates and the permeation of the electrolytic solution into the host matrix, leading to greater electrolytic connection between the TiO_2 sites. Chronopotentiometric curves and the differential capacities recorded as a function of the potential under several applied current densities indicated higher charge capacity and absorbance changes (ΔA) for the TiO_2/NOCMCh/PEO electrode. We employed the potentiostatic intermittent titration technique (PITT) to determine the chemical diffusion coefficient (D_c) associated with electron and lithium ion diffusion in the host matrices. To investigate the independent motion of these charge carriers in the absence of an internal electrical field, we also obtained the Wagner factor (W) and the lithium (D_{Li}) and electron (D_e) self-diffusion coefficients. Spectroelectrochemical measurements also indicated higher coloration front rate due to lithium ion transport in the TiO_2/NOCMCh/PEO electrodes. The electrochemical impedance spectroscopy (EIS) measurements suggested trapping effects and anomalous diffusion, which contributed to a better understanding of the role that polymeric components play in charge transport within the self-assembled materials under high electroinsertion rate.

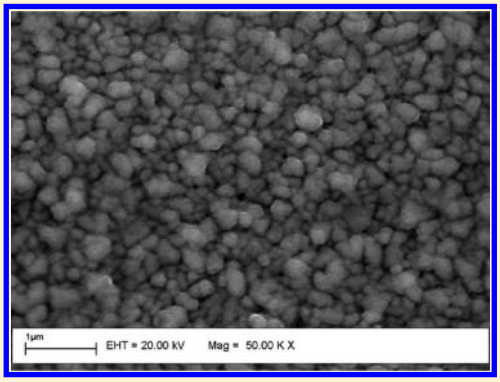

INTRODUCTION

TiO_2 has been extensively investigated due to its optical, electrical, catalytic, photocatalytic, electrochemical, and ion-exchange properties. In addition, the high chemical stability, nontoxicity, and low cost of TiO_2 have raised researchers' interest in this semiconductor material for application in several devices, such as solar cells, sensors, and photocatalytic and electrochemical devices.[1−4]

The intercalation properties of the lithium ion have also motivated scientists to investigate this material as a component of secondary batteries and electrochromic windows.[5−7] TiO_2 has high reversible capacity and is potentially applicable in the 2 V rocking-chair lithium battery, which seems to be more appropriate for microelectronic and consumer devices with photovoltaic recharging as compared with the 4 V lithium ion battery.[5−7] As for electrochromic applications, TiO_2 displays a reversible coloration change from white to blue when it is reduced upon concomitant lithium ion electroinsertion. Because this metal oxide is not a strongly colored material, it can be employed as secondary electrode in electrochromic devices.[8]

The diffusion of the guest ion within these host matrices constitutes the rate-limiting step during electroinsertion. Furthermore, not all the matrix sites are accessible. Thus, considerable effort has been made to enhance the ion diffusion rate and accessibility in these materials and to increase the charge capacity and shorten the response time of batteries and electrochromic devices.

Nanocomposites consisting of TiO_2 nanoparticles dispersed in polymeric matrices offer additional advantages as compared

Received: April 27, 2013
Revised: July 19, 2013
Published: July 23, 2013

   dx.doi.org/10.1021/jp404179x | *J. Phys. Chem. C* 2013, 117, 16774−16782

with conventional TiO_2 electrodes: their large surface area reduces the diffusion pathway during the insertion/deinsertion steps; depending on the nature and composition of these nanomaterials, highly wettable electrodes are achieved, which can boost the electrolytic connection between the TiO_2 nanoparticles and improve the access of the lithium ion to the electroactive sites as well as the diffusion rate.[9,10]

Partially dissociated alkaline salts dispersed in poly(ethylene oxide) (PEO) polymeric matrices have also been extensively studied as polymeric electrolytes.[11,12] These solids exhibit high ionic conductivity as compared with other solid materials, so they can be employed in electrochemical devices.[11] The local segmental motion of the polymeric chains in the amorphous region, above the glass transition temperature, facilitates the conductivity.[13] This polymer allows conformational changes, which favor interactions between the oxygen atoms of the CH_2CH_2O units and the lithium ions.[14]

Using the layer-by-layer (LbL) method, judiciously chosen architectures can lead to nanocomposite structures with the desired electrochemical properties. However, weak interactions between PEO and TiO_2 prevent the preparation of self-assembled films from these components. Hence, we employed *N,O*-carboxymethylchitosan (NOCMCh) to obtain a polymeric dispersion with PEO and transport the polyether into the TiO_2 self-assembled structure during the self-assembly.[15] In fact, the negative charge of the carboxyl group can establish an electrostatic interaction with positively charged TiO_2 nanoparticles, promoting the growth of uniform self-assembled films with high thickness and nanoarchitecture control. When incorporated into host matrices, NOCMCh and PEO can still be plasticized with propylene carbonate (PC), which is normally the solvent in electrolytic solutions.[16] Additionally, these polymers do not interfere in the absorbance change in the visible range of the electromagnetic spectrum and are stable in the electrochemical window used for intercalation of the lithium ion into in the TiO_2 host matrices.[17]

In this work, we investigated the lithium ion electroinsertion in the self-assembled nanocomposites prepared from TiO_2 nanoparticles, NOCMCh, and PEO. We used electrochemical methods and models to determine the physicochemical parameters associated with transport properties, which contributed to a better understanding of the role played by the polymeric components during the performance of these self-assembled electrodes under high electroinsertion rate.

EXPERIMENTAL SECTION

The TiO_2 colloidal dispersion was prepared by hydrolysis of tetra-*n*-butyl titanate acquired from Du-Pont (Tyzor).[18] A mixture of 30 mL of organic titanate and 30 mL of 2-propanol was slowly added (15 min) to 300 mL of deionized water under vigorous stirring, followed by addition of 2 mL of 70% nitric acid, also under stirring. The resulting solution was stirred for 2 h at room temperature. The mixture was then heated to 80 °C under stirring for 4 h, giving rise to a stable and transparent (slightly cloudy) TiO_2 suspension (pH = 2).

The effective diameter of the colloidal TiO_2 particles was 21.6 nm (see the size distribution histogram in Figure S1 of the Supporting Information), as determined by dynamic light scattering (DLS) in a Brookhaven Instruments Corp. The anatase phase in the films prepared by this colloidal dispersion was detected by X-ray diffraction (XRD). The XRD of the thin films, obtained after casting the TiO_2 dispersions onto the glass substrate, was recorded on a Siemens D5005 diffractometer using monochromatic Cu Kα radiation. The diffractogram displayed two diffraction peaks at 2θ values of 25° and 48°, characteristic of (101) and (200) of anatase TiO_2, respectively.[19] However, TiO_2 still presented an amorphous phase. In order to estimate the crystallinity degree of the TiO_2 nanoparticles, the areas under the diffraction peaks (A_C) and the amorphous halo (A_A) were determined, and the ratio $A_C/(A_C + A_A)$ was 63.3. The commercial PEO (MV = 100 000 g/mol) and NOCMCh (MV = 20.476 g/mol and DS = 1.5) were purchased from Aldrich and DAYANG, respectively.

LbL films were assembled onto a fluor tin oxide (FTO)-coated glass obtained from Flexitec (Curitiba, Brazil), with sheet resistance $\leq$20 Ω. The layers were achieved via ionic attraction of oppositely charged materials, by alternate immersion of the FTO substrate in TiO_2 (24 g L^{-1} and pH = 2) and NOCMCh (1.6 g L^{-1} and pH = 7) aqueous dispersions for 3 min. After deposition of each TiO_2 and NOCMCh layer, the substrates were rinsed in HCl solution for 30 s (pH = 2) and in deionized water (Milli-Q) for 30 s (pH = 7), respectively. The alternate immersion procedure was repeated 15 times, and the last layer of each LbL film was dried under nitrogen flow. The resulting material will be designated TiO_2/NOCMCh hereafter. The same procedure was carried out for the assembly of TiO_2/NOCMCh/PEO LbL films. In this case, the FTO substrate was immersed in an aqueous mixture of PEO and NOCMCh (90:10 w:w, 1.6 g dm^{-3}), followed by immersion in the TiO_2 aqueous dispersion. The dip-coating technique was applied to prepare the TiO_2 film on the FTO. The immersion and submersion rate was 10 mm min^{-1}, the substrate was kept immersed into the TiO_2 dispersion for 1 min, and the drying time was 2 min. This process was repeated, and the dip-coating films consisted of 10 layers.

The amount of titanium atoms in the LbL films was determined by spectrophotometry.[20] First, a calibration curve was constructed at 410 nm as a function of the TiO_2 concentration (from 1 to 20 mg L^{-1}) in 3 mL of H_2SO_4 and complexed with 1 mL of H_2O_2 30%. This procedure was repeated with TiO_2, TiO_2/NOCMCh, and TiO_2/NOCMCh/PEO films to determine the concentration of titanium atoms in these materials. The molar absorptivity calculated from the absorbance calibration curve at 410 nm as a function of titanium concentration was 964 mol^{-1} cm^{-1} L, and the amounts of titanium were 320 ± 7, 142 ± 3, and 220 ± 10 nmol in TiO_2, TiO_2/NOCMCh, and TiO_2/NOCMCh/PEO films, respectively.

Film thickness was analyzed by specular reflectance using the Nanocalc 2000 program coupled with a single channel 2048 pixel CCD spectrophotometer having halogen lamp as light source. The thickness values measured for the TiO_2 cast film and for the 15-bilayer TiO_2/NOCMCh and TiO_2/NOCMCh/PEO LbL films were 100 ± 4, 160 ± 4, and 140 ± 4 nm, respectively. The geometrical area of the films was 1 cm^2. Scanning electron microscopy (SEM) surface images were registered on a digital Zeiss DSM 960 microscope. The smoothing surface roughness (R_a) values for the TiO_2 film and for the 15-bilayer TiO_2/NOCMCh/PEO LbL film were 7.95 and 10.93 nm, respectively. These values were evaluated by atomic force microscopy (AFM) height images recorded on a digital Shimadzu microscope. The wettability of the films was evaluated by means of contact angle measurements using an OCA-20 Dataphysics system. To this end, 10 μL of a 0.5 mol L^{-1} $LiClO_4$/PC solution was dropped on a glass substrate

dx.doi.org/10.1021/jp404179x | J. Phys. Chem. C 2013, 117, 16774−16782

containing the film. The changes in the contact angle as a function of the time were monitored by a CCD camera. The contact angle values were acquired using Young−Laplace fitting.

For the electrochemical and spectroelectrochemical experiments, a platinum sheet with an area of 10 cm^2 and Ag/Ag^+ saturated in propylene carbonate (PC) were used as the counter electrode and the quasi-reference electrode, respectively. This quasi-reference electrode has a potential of 2.94 V versus Li/Li^+. An $LiClO_4$/PC electrolytic solution (0.5 mol L^{-1}) was employed in all the electrochemical experiments, which were carried out using an Autolab PGSTAT30 potentiostat/galvanostat. Measurements of ac electrochemical impedance spectroscopy were performed between 100 kHz and 1 mHz. Several dc potentials were accomplished with 5 mV of superimposed ac amplitude. The values of electrode bulk resistance were determined by extrapolating the impedance data obtained at high frequencies for the electrochemical cell with and without the films deposited onto the FTO substrate. Chromogenic analysis was conducted concomitant with the electrochemical experiments using a USB4000 spectrophotometer (Ocean Optics Inc.) equipped with an LS1 tungsten halogen light source and fiber optic cables with 600 μm diameter. The films were placed in a cell made of optical glass, and light beams were transmitted across the film.

RESULTS AND DISCUSSION

Figures 1a and 1b show the SEM images for the TiO_2 cast film and the 15-bilayer TiO_2/NOCMCh/PEO LbL film on the glass substrate, respectively. These images demonstrate that the materials have similar morphology and consist of aggregates with average sizes of ca. 100 and 150 nm, respectively. Considering that the thickness of these materials is in this same order of magnitude, we can suggest that nanoparticles linked to each other after solvent evaporation, to form roughly aggregates. Moreover, we can imply that the self-assembled material is not stratified. The mean size difference between these aggregates is associated with the presence of polymers; the polymers favor a higher amount of electrolytic connection between the electroinsertion sites and thus make use of a high amount of electrode material, as will be discussed below. Figure 1c depicts the SEM image of the TiO_2/NOCMCh/PEO film at higher magnification and reveals that TiO_2 nanoparticles with an average diameter of 20 nm exist in these aggregates. The TiO_2 film also contains nanoparticles with similar diameter. This average nanoparticle size is close to that measured in the TiO_2 colloidal dispersion employed in the preparation of the TiO_2/NOCMCh/PEO film.

Figures 2a and 2b display interference fringes in the visible spectra of the TiO_2/NOCMCh and TiO_2/NOCMCh/PEO films, respectively. The inset gives the absorbance as a function of the number of bilayers at 415 and 450 nm for the TiO_2/NOCMCh and TiO_2/NOCMCh/PEO films, respectively. These results evidence the role of NOCMCh in the growth of the TiO_2/NOCMCh/PEO LbL film. Moreover, we can observe a linear growth of the self-assembled TiO_2/NOCMCh/PEO film, with high thickness control and uniform TiO_2 deposition.

The contact angles after the spreading of an electrolytic solution drop on the TiO_2 and TiO_2/NOCMCh/PEO films are 23.0° and 2.3°, respectively. These results indicate lower surface energy for the electrolytic solution on the self-assembled nanocomposite compared with the TiO_2 film, which is

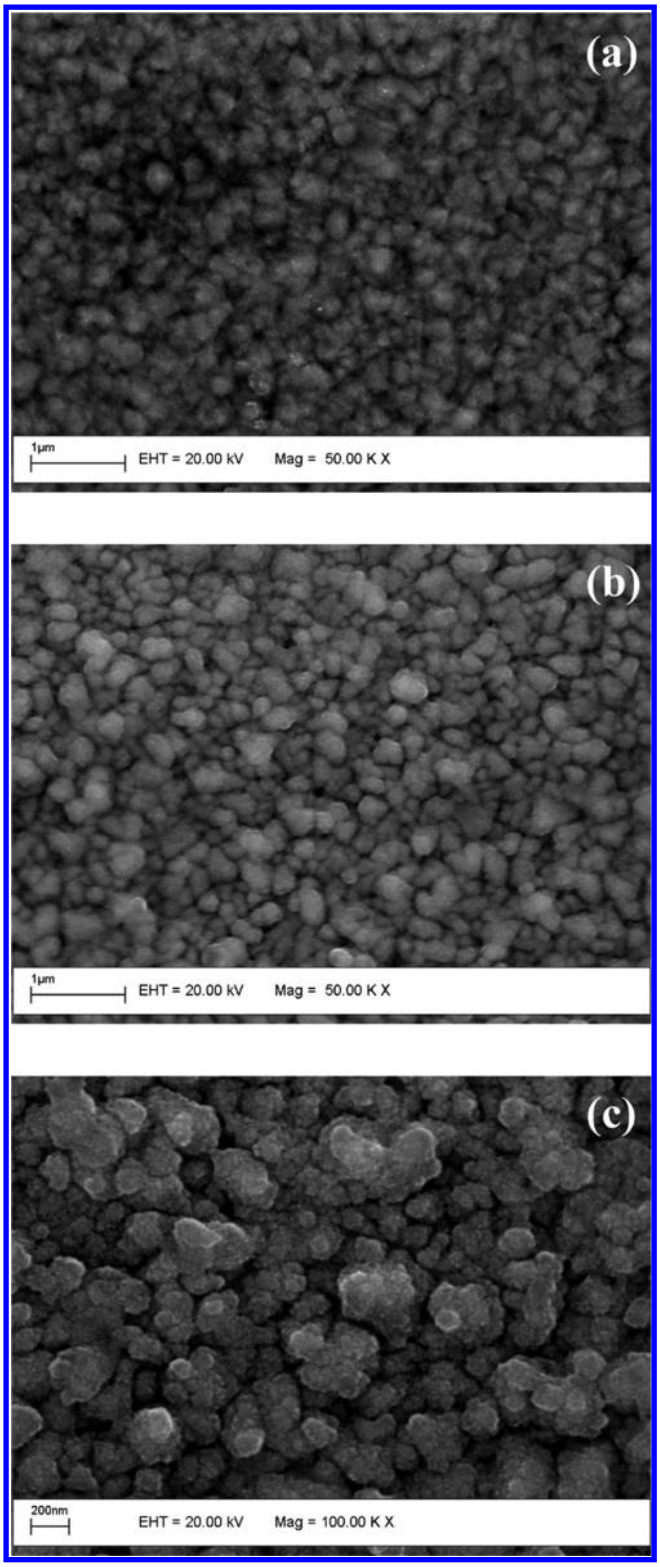

Figure 1. SEM images of the (a) TiO_2 cast film and (b) TiO_2/NOCMCh/PEO films on the glass substrate. Scale bar = 1 μm. (c) SEM image of the TiO_2/NOCMCh/PEO film at higher magnification. Scale bar = 200 nm.

associated with higher solvophilicity of the organic polymers. This favors higher $LiClO_4$/PC permeation into the self-assembled material, thereby increasing the accessibility of the lithium ions to the electroactive sites in the host matrices and ensuring higher charge capacity. Another important point is

dx.doi.org/10.1021/jp404179x | J. Phys. Chem. C 2013, 117, 16774−16782

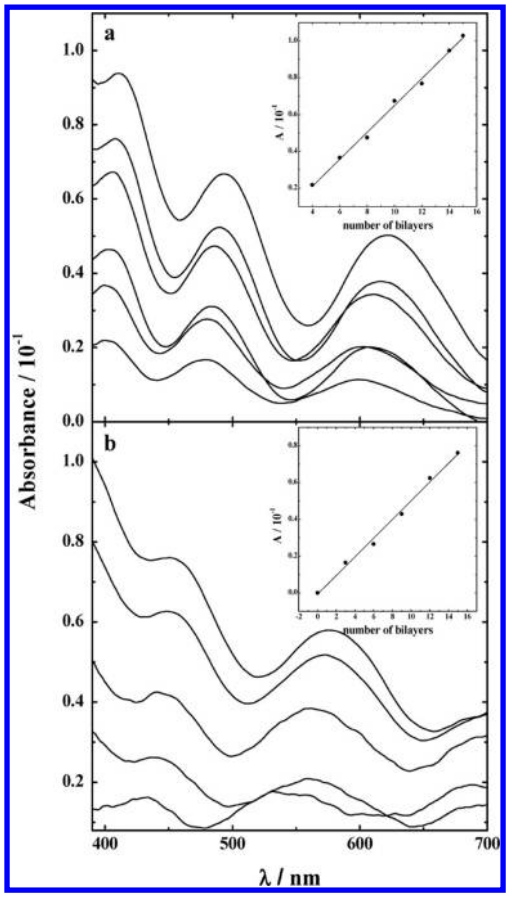

Figure 2. Visible spectra of the (a) TiO_2/NOCMCh and (b) TiO_2/NOCMCh/PEO films. Insets in (a) and (b) display the absorbance as a function of the number of bilayers at 415 and 450 nm, respectively.

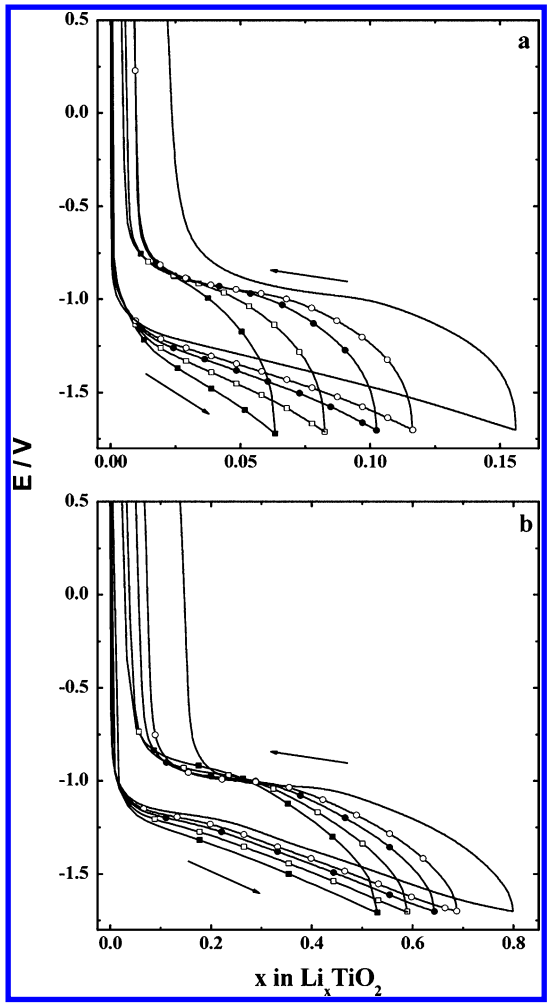

Figure 3. Charge/discharge curves for the (a) TiO_2 and (b) TiO_2/NOCMCh/PEO films at (—) 10, (○) 30, (●) 50, (□) 100, and (■) 200 μA cm^{-2}.

that the lithium ion diffusion rate rises as the host matrices are wetted, increasing the charge storage capacity, mainly under high current densities.

Figures 3a and 3b present the charge/discharge curves for the TiO_2 and TiO_2/NOCMCh/PEO films, respectively, on the FTO substrate at 10, 30, 50, 100, and 200 μA cm^{-2}. Comparing the curves obtained for the two materials, we note that the TiO_2/NOCMCh/PEO film exhibits the highest reversible stoichiometric ratio (x in Li_xTiO_2) at the cutoff potential (−1.7 V) for all the applied current densities. The highest x values diminish as a function of the current density, which is associated with lithium ion transport in the host matrices. These x values decrease from 0.16 to 0.06 mC cm^{-2} for the TiO_2 film and from 0.66 to 0.51 mC cm^{-2} for the TiO_2/NOCMCh/PEO film as the current density rises from 10 to 200 μA cm^{-2}. Considering the reversible charge and TiO_2 mass of these host matrices, the reversible specific capacities of TiO_2 and TiO_2/NOCMCh/PEO films change from 45 to 26 mA h g^{-1} and from 222 to 188 mA h g^{-1} in the applied anodic current density range, respectively. Regarding the cyclability of these electrodes, their capacities decreased on half of the initial values after 100 charge/discharge cycles (13 and 90 mA h g^{-1} for the TiO_2 and TiO_2/NOCMCh/PEO films, respectively) at 200 μA cm^{-2}.

The charge capacity of the TiO_2/NOCMCh film was also investigated. However, the x values are lower than those determined for the TiO_2/NOCMCh/PEO films, decreasing from 0.48 to 0.33 as the current density rises from 10 to 200 μA cm^{-2}. Although the cyclability of this electrode is similar to those observed for the other ones, its capacity to store charge on high lithium ion electroinsertion rate is not as good as in the case of the TiO_2/NOCMCh/PEO film.

Some authors have also used the C-rate to investigate the charge capacity as a function of current density. In our case, 1C rate corresponds to 8.6 and 3.1 μA cm^{-2} for the TiO_2 and TiO_2/NOCMCh/PEO films, respectively, which are the current densities necessary to reduce the TiO_2 sites at 1 h. Thus, the specific capacities shown above correspond to C-rates ranging from 1.2 to 23.3 and from 3.2 to 64.5 for the TiO_2 and TiO_2/NOCMCh/PEO films, respectively. On basis of these data, we can conclude that this self-assembled material has a very high charge store capacity, even under high current density or C-rates. However, we have to bear in mind the experimental conditions when comparing the high charge capacities determined in this paper with those reported by other authors. In fact, the charge storage properties depend on several experimental parameters, such as the current density, potential sweep, potential window, film thickness, nanoparticle size, and composition, among others. For example, Armstrong et al. obtained TiO_2-B nanowires with high lithium ion intercalation/deintercalation rate and high specific capacity (85 mAh g^{-1} at 3000 mA g^{-1});[21] Liu et al. produced TiO_2-B microspheres with diameter of ca. 1 μm and mesopores of 12 nm as well as

dx.doi.org/10.1021/jp404179x | J. Phys. Chem. C 2013, 117, 16774−16782

nanosized crystals of ca. 6 nm displaying fast pseudocapacitive reaction and good performance rate (116 mA h g^{-1} at 60 C).[22] The specific capacity of nanostructured TiO_2/graphene films synthesized via anionic sulfate stabilization changes from 175 to 96 mA h g^{-1} under current densities of 168 mA g^{-1} (1 C) and 5000 mA g^{-1} (30 C), respectively.[23] Anatase TiO_2 nanotubes with diameter of 10 nm and length of 200−400 nm show specific capacities of 229 and 168 mA h g^{-1} under current densities of 36 mA g^{-1} (≈1.6 C) and 210 mA g^{-1} (≈9.2 C), respectively.[24] The values of specific capacity determined for the nanocomposite in this paper are higher than those verified for anatase nanoparticles with a diameter of 5 nm (48 mA h g^{-1} at 30 C), anatase mesoporous particles (ca. 10 mA h g^{-1} at 30 C), and nanoparticles with 300 nm (ca. 10 mA h g^{-1} at 5 C).[10]

Figures 4a and 4b represent the differential capacities (dx/dE) as a function of the potential for the TiO_2 and TiO_2/NOCMCh/PEO films, respectively, on the FTO substrate at 50 and 200 μA cm^{-2}, obtained from the chronopotentiometric curves. During the reduction process at 50 μA cm^{-2}, a dx/dE peak appears at −1.21 V for the TiO_2/NOCMCh/PEO film, whereas the TiO_2 film displays only a large dx/dE peak at −1.39 V. These peaks shift to less positive potentials at higher current densities due to low lithium ion mobility; moreover, these peaks appear at more negative potentials for the TiO_2 film compared with the self-assembled films. Furthermore, the dx/dE peak observed during the oxidation process is higher and narrower for the self-assembled material. These results suggest that the presence of NOCMCh and PEO can increase the lithium ion mobility between the TiO_2 nanoparticles.

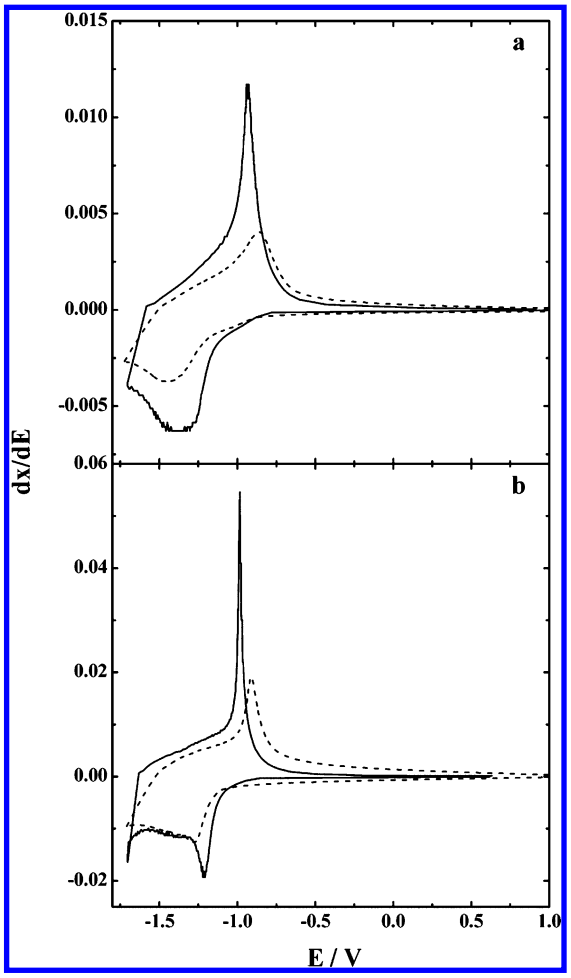

Figure 4. Differential capacities (dx/dE) as a function of the potential for the (a) TiO_2 and (b) TiO_2/NOCMCh/PEO film at (—) 50 and (- - -) 200 μA cm^{-2}.

We used the potentiostatic intermittent titration technique (PITT) to calculate the chemical diffusion coefficients (D_c) in these host matrices and to investigate the mass transport properties during lithium ion electroinsertion.[25] We applied 50 mV potential steps and allowed the current density to diminish to values close to zero. We repeated this procedure five times, using different potentials (from −1.25 to −1.5 V) and injected charges. Figure 5a displays the stoichiometric ratio as a function of the time square root during the potential step (between −1.3 and −1.35 V, in this case). We computed the D_c values according to the equation

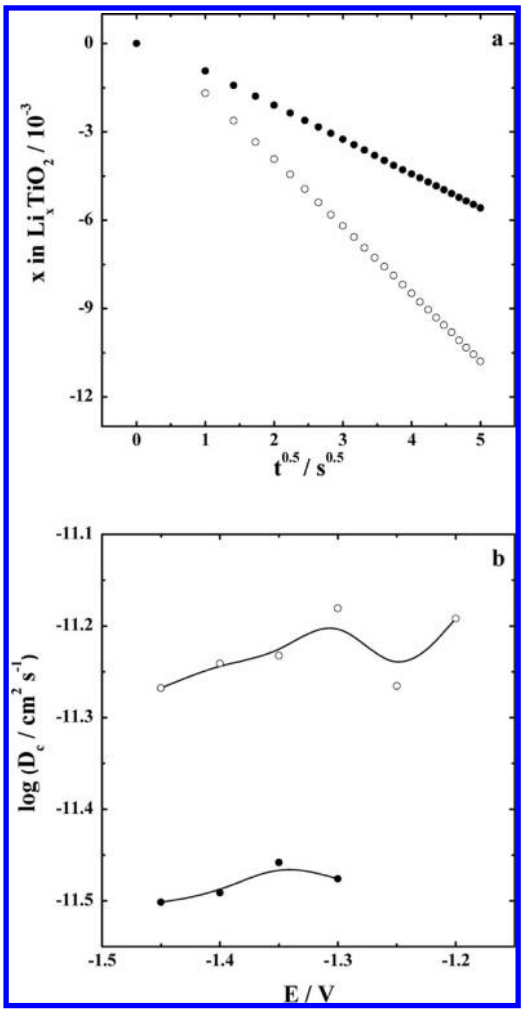

Figure 5. (a) Stoichiometric ratio (x in Li_xTiO_2) as a function of the time square root. (b) D_c values as a function of the potential for the (●) TiO_2 and (○) TiO_2/NOCMCh/PEO films.

$$D_c = \left(\frac{dx}{d\sqrt{t}}\frac{L}{2\Delta x}\right)^2 \pi \quad (1)$$

where L is the thickness of the materials, the dx/d$t^{0.5}$ term is the slope of the stoichiometric ratio x as a function of the time square root during each potential step, and Δx is the stoichiometric ratio change during the same potential steps. The injected charge little affects the D_c values (Figure 5b).

dx.doi.org/10.1021/jp404179x | J. Phys. Chem. C 2013, 117, 16774−16782

These coefficients are close to 3.0×10^{-12} and 6.5×10^{-12} cm^2 s^{-1} for the TiO_2 and TiO_2/NOCMCh/PEO films, respectively. These results indicate that PEO slightly modifies the lithium ion diffusion rate from −1.3 to −1.5 V. This phenomenon can also be associated with the intimate contact between the solvophilic polymeric chains and the TiO_2 nanoparticles, which increased the solvent permeation into the nanocomposites, thereby enhancing the ionic mobility.[26] However, the difference between these D_c values is not sufficient to justify a much higher diffusion rate and charge capacity for the TiO_2/NOCMCh/PEO film compared with the TiO_2 electrode, suggesting that the accessibility to electroactive sites promoted by these polymers also increases the charge capacity. Moreover, lithium ion trapping effects influence the electrochemical response during the electroinsertion process at less negative potentials, as will be shown below.

Figure 6a displays the absorbance change (ΔA) as a function of the injected charge (q) for the TiO_2 and TiO_2/NOCMCh/PEO films on the FTO substrate at 50 μA cm^{-2}, as obtained from monochromatic incident radiation at 660 nm during the charge/discharge experiments shown in Figure 3. We determined the electrochromic efficiency of these materials on the basis of the slope of these curves (ca. 18 cm^2 C^{-1} for the two materials investigated in this work). Our data indicate that the polymers present in the self-assembled nanocomposite do not interfere in the optical properties or promote parallel reactions during the lithium ion insertion/deinsertion. Figure 6b shows the derivative dA/dE as a function of the potential for the two films at 50 μA cm^{-2}, obtained from the chronopotentiometric curves. Note that the profile of these curves is similar to those shown in Figure 3, indicating that the potentials of the dx/dE peak are associated exclusively with reduction/oxidation of Ti^{4+}/Ti^{3+} and that the organic polymers do not participate in the redox process. Moreover, the dA/dE peaks observed during the deinsertion process are sharper and intense for the self-assembled material as compared with the TiO_2 film. These results suggest higher coloration front rate for the electrochromic self-assembled films as submitted to potential changes.

Since the lithium ion diffusion in the host matrix is the rate-limiting step, and knowing that the lithium ion and the electron move together to maintain electroneutrality, we used a spectroelectrochemical method to calculate the optical diffusion coefficients (D_{op}) in these host matrices, based on the potentiostatic intermittent titration technique (PITT). Figure 6c illustrates the absorbance change (at 660 nm) as a function of the time square root, which we recorded during the potential steps between −1.30 and −1.35 V. In this case, we used the following equation to calculate D_{op}

$$D_{op} = \left(\frac{d\Delta A}{d\sqrt{t}}\frac{L}{2\Delta A}\right)^2 \pi \qquad (2)$$

where the $d(\Delta A)/dt^{0.5}$ term is the slope of the absorbance change as a function of the time square root during each potential step and ΔA is the absorbance change during the same potential steps. The D_{op} values are 3.1×10^{-12} and 6.2×10^{-12} cm^2 s^{-1} for the TiO_2 and TiO_2/NOCMCh/PEO films, respectively. The D_{op} values helped us confirm the lowest response time of absorbance changes and the highest coloration front rate for the self-assembled films; these values are close to the D_c values, reinforcing that the polymers affect lithium ion diffusion.

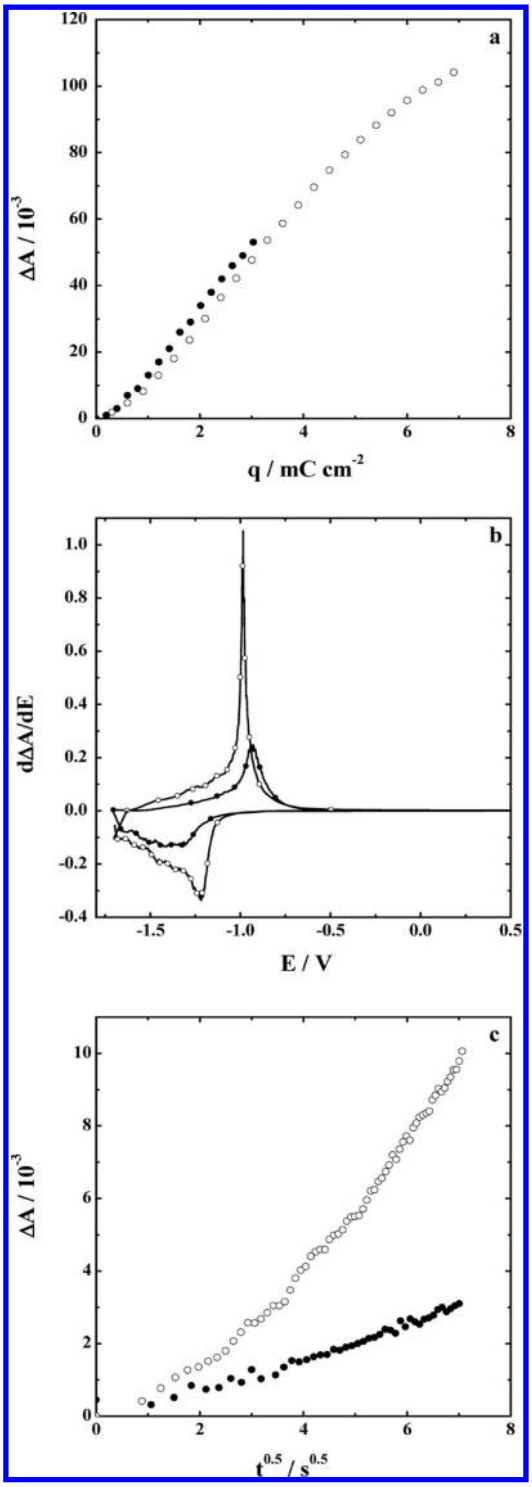

Figure 6. (a) Absorbance change (ΔA) as a function of the injected charge (q). (b) $d\Delta A/dE$ values as a function of the potential during the chronopotentiometric experiments at 50 μA cm^{-2}. (c) Absorbance change (ΔA) as a function of the time square root during the potential steps between −1.30 and −1.35 V for (●) TiO_2 and (○) TiO_2/NOCMCh/PEO films at 660 nm.

The lithium ion self-diffusion coefficient (D_{Li}) values can be determined according to the equation[27]

$$D_{Li} = \frac{RT}{F}\left(\frac{dx}{dE}\right)D_c \qquad (3)$$

dx.doi.org/10.1021/jp404179x | J. Phys. Chem. C 2013, 117, 16774−16782

where dx/dE is the slope of the stoichiometric ratio x as a function of the equilibrium potential. Although the D_c values do not differ significantly, the D_{Li} values are a half-order of magnitude larger for TiO_2/NOCMCh/PEO compared with the TiO_2 film at low potentials (Figure 7a). Thus, PEO and modified chitosan influence the ionic diffusion when these ions move independently of electron displacement in the TiO_2 conduction band. The Wagner (W) factor determined from the D_c/D_{Li} ratio changed from ca. 146 to 107 and from ca. 320 to 53 for the TiO_2 and TiO_2/NOCMCh/PEO films, respectively (Figure 7b). These W values indicate that, at more negative potentials, the internal electric field between the charge carriers accelerates more the lithium ion in the TiO_2 film than in the self-assembled films, as will be discussed below.

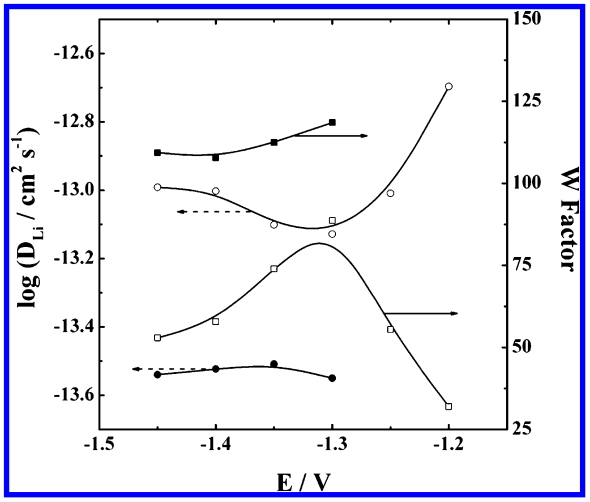

Figure 7. D_{Li} values for the (●) TiO_2 and (○) TiO_2/NOCMCh/PEO films and W factor values for the (■) TiO_2 and (□) TiO_2/NOCMCh/PEO films as a function of the potential.

Figures 8a,b and 8c,d contain the complex capacitance diagrams for TiO_2 and TiO_2/NOCMCh/PEO films, respectively, at two dc potentials: −1.25 V (a, c) and −1.5 V (b, d). In Figure 8a, the semicircle at high frequencies corresponds to lithium ion electroinsertion at the TiO_2 film/electrolytic solution interface. Meanwhile, the semicircle at low frequencies refers to lithium ions trapped in the host matrix. Energy barriers of different heights exist in the ionic diffusion pathway.[28] Thus, in some sites (trapping sites), the lithium ions take longer to overcome high energy barriers than in other sites (diffusion sites).[29] On the other hand, the complex capacitance diagrams for TiO_2 at −1.5 V and for the self-assembled materials display a semicircle at high frequencies associated with charge transfer at the film/electrolytic solution interface and a straight line with a constant phase angle which characterizes the lithium ion semi-infinite diffusion in the host matrices. This behavior indicates higher ionic delocalization than in the case of ionic trapping.

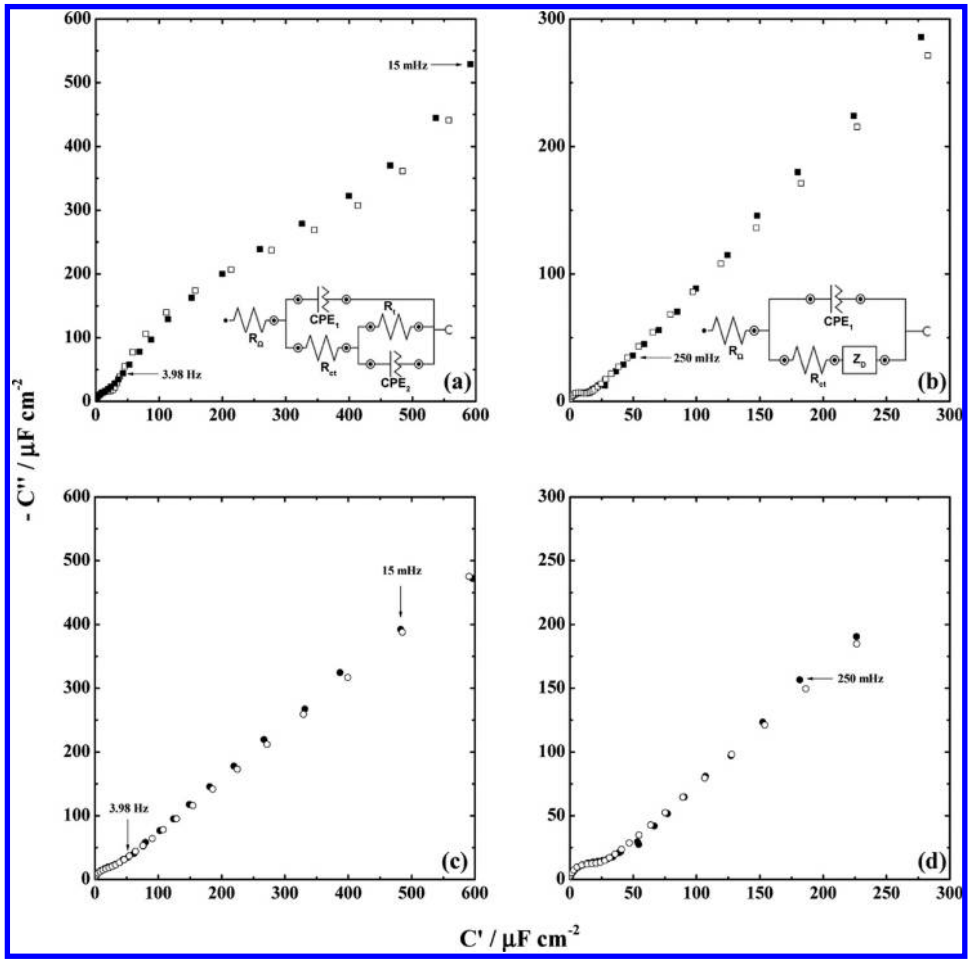

Figure 8. Complex capacitance diagrams for TiO_2 at (a) −1.25 V and (b) −1.5 V (■, experimental; □, theoretical) and for TiO_2/NOCMCh/PEO at (c) −1.25 V and (d) −1.5 V (●, experimental; ○, theoretical).

dx.doi.org/10.1021/jp404179x | J. Phys. Chem. C 2013, 117, 16774−16782

The fitting of the complex capacitance diagrams shown in Figure 8a is based on the equivalent circuit shown in the inset of the same Figure 8a, where R_Ω is the sum of electrolytic solution, substrate, and electrode bulk (R_b) resistances, R_{ct} is the charge transfer resistance, and R_t is the trapping resistance. Constant phase elements 1 and 2 (CPE1 and CPE2) represent the charging of the electrical double layer and trapping effects in the electrode bulk, respectively, due to frequency dispersions associated with the surface roughness and height distribution of the energy barrier in the ionic diffusion pathway. $Z_{CPE1} = 1/Q_1(j\omega)^n$ and $Z_{CPE2} = 1/Q_2(j\omega)^n$ refer to the impedances of CPE1 and CPE2, respectively, where Q_1 and Q_2 are constants with dimension Fs^{n-1}. Meanwhile, the inset in Figure 8b displays the equivalent circuit used to fit the other complex capacitance diagrams, where Z_D represents the impedance associated with the semi-infinite diffusion.

Based on the D_{Li} values determined above, electron self-diffusion coefficients can also be determined on the basis of diffusion models for charge carriers in bulk films.[30] Considering the frequency dispersion associated with lithium ion diffusion, we also used the model of anomalous diffusion, according to which the mean-square displacement of the diffusing species follows a power law dependence on time.[31] In this case, the number of lithium ions diffusing in the host matrices is not conserved. Thus, the second Fick's law becomes

$$\frac{\partial^\gamma C_{Li}}{\partial t^\gamma} = -\frac{\partial J}{\partial z} \tag{4}$$

where C_{Li} is the concentration of lithium ions in the host matrix, z is the position, and γ is a dimensionless parameter lower than 1. Based on the model proposed by Vorotyntsev et al.[30] and with the following electron (J_e) and lithium ion (J_{Li}) fluxes at the interfaces (where I is the current and e is the elementar charge)

$$J_e = -I/eJ_{Li} = 0 \quad \text{at } z = 0 \tag{5}$$

$$J_{Li} = I/eJ_e = 0 \quad \text{at } z = L \tag{6}$$

we employed eqs 7 and 8 to fit the capacitance diagrams. Then, we determined the D_e values, where i is the imaginary unit.

$$Z_D = R_b \frac{D_e}{2D_{Li}} \frac{\tanh 2\nu}{\nu} \tag{7}$$

$$\nu = \left(\frac{L^2}{8D_{Li}}\right)^{1/2} (i\omega)^{\gamma/2} \tag{8}$$

The values of R_b used to calculate the Z_D values in eq 7 were ca. 1 Ω cm^2 for both electrodes, determined according to the Experimental Section. The magnitude of Q_1 values (20 μF cm^{-2} for both electrodes) indicates that the electrochemical process associated with the semicircle at high frequencies really relates to the electrode/electrolytic solution interface, once the double layer capacitance is normally close to these values. In contrast, the Q_2 values (399 μF cm^{-2} for the TiO_2 film) suggest that capacitive processes take place in the bulk electrode, as a result of the trapping effects (R_t = 30 kΩ cm^{-2} for TiO_2). This trapping tends to decrease the ionic mobility in the host matrices, explains the electrochemical profile of dx/dE peaks and probably diminishes the charge capacity of the TiO_2 film.

Although the presence of NOCMCh and PEO tends to hamper the lithium ion and electron transport at the electrode surface and bulk, respectively, these polymers do not interfere in these properties significantly. Indeed, the electrodes investigated here have similar R_{ct} (70 and 80 Ω for TiO_2 and TiO_2/NOCMCh/PEO at −1.5 V, respectively) and D_e values (≈2.0 × 10^{-8} cm^2 s^{-1} for both materials at −1.5 V). Therefore, these polymers act mainly on the lithium ion transport and lithium accessibility to the electroactive sites. Finally, these similar D_e values also suggest that the highest W values (at more negative potentials) observed for the TiO_2 film relate to the lowest D_{Li} values determined for this electrode. Moreover, these D_e values show that the electronic transport in the nanocomposites does not hinder the enhancement in the lithium ion motion associated with the internal electric field. On the basis of the D_c, D_{Li}, D_e, and W values determined in this paper, the inclusion of electronic conducting components in these self-assembled materials (to increase the Wagner factor values) can further increase the lithium ion mobility and, consequently, the charge capacity.

CONCLUSIONS

Because it was not possible to prepare LbL films formed from PEO and TiO_2, we incorporated the ionic conductor polymer into the self-assembled structure of TiO_2 nanoparticles using NOCMCh and PEO polymeric dispersion. This allowed visually homogeneous nanocomposites with high thickness control to grow spontaneously. Based on charge/discharge curves, the charge capacity of the TiO_2/NOCMCh/PEO film was higher than that of the TiO_2 film under high electroinsertion rate. The surface tension of the electrolytic solution decreased for the self-assembled TiO_2/NOCMCh/PEO film compared with the TiO_2 film, suggesting higher solvent permeation into the self-assembled structure. This probably improved lithium ion mobility and accessibility to the electroactive sites. In the case of the self-assembled nanocomposite, we did not detect the lithium ion trapping effect during the electroinsertion taking place throughout the chronopotentiometric experiments. Moreover, the R_b and D_e values indicated that NOCMCh and PEO virtually do not hinder the electron transport between the TiO_2 nanoparticles in the nanocomposites, guaranteeing the lithium ion motion due to the internal electric field generated between the electron−lithium ion pair. Moreover, the presence of these polymers did not significantly contribute to the ohmic drop during the lithium ion electroinsertion. These factors increased the optical diffusion coefficient, suggesting enhanced coloration wave rate and shorter electrochromic response time. Considering the parameters determined in this article, the self-assembled material investigated here can be an alternative for several applications involving lithium ion electroinsertion under high intercalation rate.

ASSOCIATED CONTENT

Supporting Information

Figure showing the size distribution histogram of the colloidal TiO_2 nanoparticles. This material is available free of charge via the Internet at http://pubs.acs.org.

AUTHOR INFORMATION

Corresponding Author

*Phone +55-16-3602-4862; e-mail fritz@ffclrp.usp.br (F.H.).

Notes

The authors declare no competing financial interest.

■ ACKNOWLEDGMENTS

We are grateful to FAPESP (Projects 2009/14181-1 and 2011/21545-0), NanoBiotec-Brasil (CAPES), and INCT-ADAPTA/FAPEAM/CNPq (573976/2008-2) for financial support. We are also grateful to Prof. Rogéria Rocha Gonçalves and Prof. Maria Elisabete Darbello Zaniquelli for allocation of their laboratory premises. We also thank Prof. Ana Paula Ramos for contact angle measurements.

■ REFERENCES

(1) Nishikiori, H.; Uesugi, Y.; Setiawan, R. A.; Fujii, T.; Qian, W.; El-Sayed, M. A. Photoelectric Conversion Properties of Dye-Sensitized Solar Cells Using Dye-Dispersing Titania. *J. Phys. Chem. C* **2012**, *116*, 4848−4854.

(2) Zimny, K.; Rogues-Cannes, T.; Carteret, C.; Stebe, M. J.; Blin, J. L. Synthesis and Photoactivity of Ordered Mesoporous Titania with a Semicrystalline Framework. *J. Phys. Chem. C* **2012**, *116*, 6585−6594.

(3) Gratzel, M. Sol-Gel Processed TiO_2 Films for Photovoltaic Applications. *J. Sol-Gel Sci. Technol.* **2001**, *22*, 7−13.

(4) Wu, C.-H.; Hsu, C.-Y.; Huang, K.-C.; Nien, P.-C.; Lin, J.-T. s.; Ho, K.-C. A Photoelectrochromic Device Based on Gel Electrolyte with a Fast Switching Rate. *Sol. Energy Mater. Sol. Cells* **2012**, *99*, 148−153.

(5) Panda, S. K.; Yoon, Y.; Jung, H. S.; Yoon, W.-S.; Shin, H. Nanoscale Size Effect of Titania (Anatase) Nanotubes with Uniform Wall Thickness As High Performance Anode for Lithium-Ion Secondary Battery. *J. Power Sources* **2012**, *204*, 162−167.

(6) Exnar, I.; Kavan, L.; Huang, S. Y.; Gratzel, M. Novel 2 V Rocking-Chair Lithium Battery Based on Nano-crystalline Titanium Dioxide. *J. Power Sources* **1997**, *68*, 720−722.

(7) Jang, H.; Suzuki, S.; Miyayama, M. Synthesis of Open Tunnel-Structured TiO_2(B) by Nanosheets Processes and Its Electrode Properties for Li-Ion Secondary Batteries. *J. Power Sources* **2012**, *203*, 97−102.

(8) Monk, P. M. S.; Mortimer, R. J.; Rossinsky, D. R. *Electrochromism: Fundamentals and Applications*; VCH: New York, 1995; p 239.

(9) Su, X.; Wu, Q.; Zhan, X.; Wu, J.; Wei, S.; Guo, Z. Advanced Titania Nanostructures and Composites for Lithium Ion Battery. *J. Mater. Sci.* **2012**, *47*, 2519−2534.

(10) Guo, Y. G.; Hu, Y. S.; Sigle, W.; Maier, J. Superior Electrode Performance of Nanostructured Mesoporous TiO_2 (Anatase) through Efficient Hierarchical Mixed Conducting Networks. *Adv. Mater.* **2007**, *19*, 2087−2091.

(11) Armand, M. The History of Polymer Electrolytes. *Solid State Ionics* **1994**, *69*, 309−319.

(12) Fenton, D. E.; Parker, J. M.; Wright, P. V. Complexes of Alkali-Metal Ions with Poly(Ethylene Oxide). *Polymer* **1973**, *14*, 589−589.

(13) Croce, F.; Appetecchi, G. B.; Persi, L.; Scrosati, B. Nanocomposite Polymer Electrolytes for Lithium Batteries. *Nature* **1998**, *394*, 456−458.

(14) Armand, M. Polymer Solid Electrolytes - an Overview. *Solid State Ionics* **1983**, *9−10*, 745−754.

(15) Chen, X.; Liu, Y.; Shi, H.; Wang, X.; Qi, K.; Zhou, X.; Xin, J. H. Carboxymethyl Chitosan Coating to Block Photocatalytic Activity of TiO_2 Nanoparticles. *Text. Res. J.* **2010**, *80*, 2214−2222.

(16) Kim, Y. T.; Smotkin, E. S. The Effect of Plasticizers on Transport and Electrochemical Properties of PEO-Based Electrolytes for Lithium Rechargeable Batteries. *Solid State Ionics* **2002**, *149*, 29−37.

(17) Galiote, N. A.; Parreira, R. L. T.; Rosolen, J. M.; Huguenin, F. Self-Assembled Films from WO_3: Electrochromism and Lithium Ion Diffusion. *Electrochem. Commun.* **2010**, *12*, 733−736.

(18) Huguenin, F.; Zucolotto, V.; Carvalho, A. J. F.; Gonzalez, E. R.; Oliveira, O. N. Layer-by-Layer Hybrid Films Incorporating WO_3, TiO_2, and Chitosan. *Chem. Mater.* **2005**, *17*, 6739−6745.

(19) Tebby, Z.; Babot, O.; Toupance, T.; Park, D.-H.; Campet, G.; Delville, M.-H. l. n. Low-Temperature UV-Processing of Nanocrystalline Nanoporous Thin TiO_2 Films: An Original Route toward Plastic Electrochromic Systems. *Chem. Mater.* **2008**, *20*, 7260−7267.

(20) Kus, S.; Marczenko, Z.; Obarski, N. Determination of Titanium with Hydrogen-Peroxide in Steels Using Derivative Spectrophotometry. *Chem. Anal. (Warsaw, Pol.)* **1992**, *37*, 569−578.

(21) Armstrong, A. R.; Armstrong, G.; Canales, J.; Garcia, R.; Bruce, P. G. Lithium-Ion Intercalation into TiO_2-B Nanowires. *Adv. Mater.* **2005**, *17*, 862−865.

(22) Liu, H.; Bi, Z.; Sun, X. G.; Unocic, R. R.; Paranthaman, M. P.; Dai, S.; Brown, G. M. Mesoporous TiO_2-B Microspheres with Superior Rate Performance for Lithium Ion Batteries. *Adv. Mater.* **2011**, *23*, 3450−3454.

(23) Wang, D.; Choi, D.; Li, J.; Yang, Z.; Nie, Z.; Kou, R.; Hu, D.; Wang, C.; Saraf, L. V.; Zhang, J.; et al. Self-Assembled TiO_2−Graphene Hybrid Nanostructures for Enhanced Li-Ion Insertion. *ACS Nano* **2009**, *3*, 907−914.

(24) Xu, J.; Jia, C.; Cao, B.; Zhang, W. F. Electrochemical Properties of Anatase TiO_2 Nanotubes as an Anode Material for Lithium-Ion Batteries. *Electrochim. Acta* **2007**, *52*, 8044−8047.

(25) Wen, C. J.; Boukamp, B. A.; Huggins, R. A.; Weppner, W. Thermodynamic and Mass-Transport Properties of Lial. *J. Electrochem. Soc.* **1979**, *126*, 2258−2266.

(26) Galiote, N. A.; Camargo, M. N. L.; Iost, R. M.; Crespilho, F.; Huguenin, F. Effects of Self-Assembled Materials Prepared from V_2O_5 for Lithium Ion Electroinsertion. *Langmuir* **2011**, *27*, 12209−12217.

(27) Weppner, W.; Huggins, R. A. Determination of Kinetic-Parameters of Mixed-Conducting Electrodes and Application to System Li_3Sb. *J. Electrochem. Soc.* **1977**, *124*, 1569−1578.

(28) Galiote, N. A.; Carvalho, A. J. F.; Huguenin, F. Trapping of Charge Carriers in Colloidal Particles of Self-Assembled Films from TiO_2 and Poly(vinyl sulfonic acid). *J. Phys. Chem. B* **2006**, *110*, 24612−24620.

(29) Bisquert, J. Analysis of the Kinetics of Ion Intercalation - Ion Trapping Approach to Solid-State Relaxation Processes. *Electrochim. Acta* **2002**, *47*, 2435−2449.

(30) Vorotyntsev, M. A.; Daikhin, L. I.; Levi, M. D. Modeling the Impedance Properties of Electrodes Coated with Electroactive Polymer-Films. *J. Electroanal. Chem.* **1994**, *364*, 37−49.

(31) Bisquert, J.; Compte, A. Theory of the Electrochemical Impedance of Anomalous Diffusion. *J. Electroanal. Chem.* **2001**, *499*, 112−120.